

NEXXUS: A comprehensive ROSAT survey of coronal X-ray emission among nearby solar-like stars [★]

J. H. M. M. Schmitt and C. Liefke

Hamburger Sternwarte, Universität Hamburg, Gojenbergsweg 112, D-21029 Hamburg, Germany
e-mail: jschmitt@hs.uni-hamburg.de; cliefke@hs.uni-hamburg.de

Received 19 February 2003 / Accepted 20 March 2003

Abstract. We present a final summary of all ROSAT X-ray observations of nearby stars. All available ROSAT observations with the ROSAT PSPC, HRI and WFC have been matched with the CNS4 catalog of nearby stars and the results gathered in the Nearby X-ray and XUV-emitting Stars data base, available via www from the Home Page of the Hamburger Sternwarte at the URL <http://www.hs.uni-hamburg.de/DE/For/Gal/Xgroup/nexxus>. New volume-limited samples of F/G-stars ($d_{lim} = 14$ pc), K-stars ($d_{lim} = 12$ pc), and M-stars ($d_{lim} = 6$ pc) are constructed within which detection rates of more than 90 % are obtained; only one star (GJ 1002) remains undetected in a pointed follow-up observation. F/G-stars, K-stars and M-stars have indistinguishable surface X-ray flux distributions, and the lower envelope of the observed distribution at $F_X \approx 10^4$ erg/cm²/sec is the X-ray flux level observed in solar coronal holes. Large amplitude variations in X-ray flux are uncommon for solar-like stars, but maybe more common for stars near the bottom of the main sequence; a large amplitude flare is reported for the M star LHS 288. Long term X-ray light curves are presented for α Cen A/B and Gl 86, showing variations on time scales of weeks and demonstrating that α Cen B is a flare star.

Key words. stars: activity – stars: coronae – stars: late type – X-rays: stars

1. Introduction

The discovery of X-ray emission from normal stars with the *Einstein Observatory* (Vaiana et al. 1981) and ROSAT demonstrated the ubiquity of hot coronae around late-type stars. Specifically, the volume-limited surveys by Schmitt et al. (1995) and Schmitt (1997) showed that coronal formation is universal in the sense that coronae are formed basically for all (or almost all) main-sequence stars with outer convection zones. Furthermore, the state of “minimum energy” of a stellar corona (around a main sequence star) was found to be one whose mean X-ray surface flux corresponds to the surface flux of a solar coronal hole. Hünsch et al. (1999) and Sterzik & Schmitt (1997) extended those studies to all stars within 25 pc by cross-correlating the ROSAT all-sky survey (RASS) data with entries in the Gliese catalog (CNS3) of nearby stars and detected a significant fraction of stars listed in CNS3 as X-ray sources in the all-sky survey data, while Hünsch et al. (1998b) and Hünsch et al. (1998a) carried out similar studies for bright main sequence and giant stars in the Bright Star Catalog and Schröder et al. (1998)

presented a volume-limited sample of giant stars within 35 pc around the Sun. Similar studies on early-type stars were presented by Berghöfer et al. (1997), who present a catalog of bright O- and B-type stars detected in the ROSAT all-sky survey, while Fleming et al. (1996) discuss X-ray emitting white dwarfs detected in the ROSAT all-sky survey. The dearth of X-ray emission among A-type stars has already been noted on the basis of observations with the *Einstein Observatory* (Schmitt et al. 1985), Hünsch (2001) presents a similar study from the ROSAT all-sky survey data, and Simon et al. (1995) from pointed ROSAT data. As to open clusters, most of them are too distant for sensitive studies with ROSAT survey data, so most of the ROSAT work on open clusters was carried using pointing data; for an overview of this work see (Randich 2000). The Hyades cluster, however, has very a large angular extent because of its proximity and can be comprehensively studied only with survey data. Stern et al. (1995) present the as of to date most complete X-ray study of the Hyades, while Schmitt et al. (1993) present the ROSAT all-sky survey data on the core of the Pleiades cluster.

One of the key properties of late-type stars is their X-ray variability. The ROSAT all-sky survey with its approximately 30 sec snapshot exposures extending over two days and longer provided a unique sampling pattern of coronal X-ray emission. In particular, long-duration flares

Send offprint requests to: J.H.M.M. Schmitt

[★] Tables 1-3 are also available in electronic form at the CDS via anonymous ftp to <cdsarc.u-strasbg.fr> (130.79.128.5) or via <http://cdsweb.u-strasbg.fr/cgi-bin/qcat?J/A+A/>

and rotational modulation can be well studied with such data. Schmitt (1994) discusses ROSAT survey observations of flare stars, and Haisch & Schmitt (1994) study specifically the X-ray variability of giants observed during the all-sky survey. Fuhrmeister & Schmitt (2003) present a systematic study of X-ray variability in the RASS data, finding that stars are indeed the most variable class of X-ray emitters.

Meanwhile the ROSAT operations have ended and no further ROSAT data will be taken. Data from numerous individual pointings in particular with the ROSAT HRI have become available in the ROSAT archive, the ROSAT survey data have been reprocessed, and the Gliese catalog of nearby stars has been substantially updated. The purpose of this paper is therefore to revisit and supplement the studies by Schmitt (1997) and Sterzik & Schmitt (1997) by utilizing all available – and presumably final since reprocessed – ROSAT data. Specifically, Schmitt et al. (1995), Schmitt (1997) and Sterzik & Schmitt (1997) had to use the pre-HIPPARCOS distance scale, but far more accurate HIPPARCOS parallaxes are now available for many nearby stars. Interestingly, the parallaxes for the brighter stars tended to be “older” hence less reliable so that the composition of the volume-limited samples has changed. Further, the ongoing infrared all-sky surveys provide “new” stars even in the immediate solar vicinity. Especially for K-type stars more ROSAT data on nearby stars were taken during the last years of its lifetime. In summary, now appears to be a good opportunity for a definitive summary of all ROSAT observations of nearby stars.

2. Observations

The ROSAT Observatory was operated between 1990 - 1998. Between July 1990 and January 1991 it carried out its ROSAT All-Sky Survey (RASS) with the ROSAT Position Sensitive Proportional Counter (PSPC). Afterwards pointed observations of individual X-ray sources were carried out in the framework of the ROSAT guest investigator program both with the PSPC and a High (angular) Resolution Imager (HRI). These detectors had fields of view of about 7000 arcmin^2 for the PSPC and 1000 arcmin^2 for the HRI, so that many X-ray sources were picked up serendipitously in the field of view of many observations whose original scientific goal was actually quite different. A boron filter could be placed in front of the PSPC detector for pointed observations allowing to separate the X-ray band below 0.28 keV (i.e., the “carbon” band) into two separate energy bands; however, only a rather small number of observations was carried out with the boron filter in place.

2.1. X-ray data

The results of both the RASS observations and the ROSAT pointed observations are available in the ROSAT results archive in the form of source lists. All five source

catalogs used for this study, i.e. the ROSAT Bright Source and Faint Source Catalog, the Second ROSAT Source Catalog of Pointed Observations with the PSPC with and without filter and the First ROSAT Source Catalog of Pointed Observations with the HRI as well as detailed information on the detection and screening procedures applied in the construction of the catalogs are available via www from the ROSAT Home Page at Max-Planck-Institut für Extraterrestrische Physik <http://wave.xray.mpe.mpg.de/rosat/catalogue> or its mirror sites. These catalogs were our primary source of information, and only in individual cases (discussed explicitly in our paper) did we go back to the original X-ray data. It is important to realize in this context that the above source catalogs have been constructed with rather conservative detection thresholds. The use of these conservative thresholds was mandatory since X-ray sources were searched for everywhere in all the ROSAT images. Since we are interested in X-ray emission only from specific locations (i.e., at the positions of nearby stars), we are working with a far smaller number of trial positions and can therefore “afford” choosing lower acceptance thresholds without compromising on the number of spurious sources. It is therefore possible in principle to obtain X-ray “detections” from stars not listed in the above catalogs and in our data base; specific cases discussed below are the nearby K star Gl 653 and the nearby M-dwarf LHS 288 .

2.2. Optical data

As our source of optical data we used the CNS4 compilation of nearby stars compiled by Jahreiss (2002). As pointed out above, the ongoing ever more sensitive infrared surveys provide “new” stars in the immediate vicinity of the Sun such as the M9V dwarf DENIS-P J104814.7-395606.1 at a distance of possibly $4.1 \pm 0.6 \text{ pc}$ (Delfosse et al. 2001) or LHS 2090 (Scholz et al. 2001), although very often the parallax information on those stars is extremely limited. Therefore no compilation of nearby stars can be truly complete. Still, among the F, G and K type stars the CNS4 catalog ought to be complete and the only source of error should be the parallax error which can move a given star outside or inside a specified sampling volume. On the other hand, among the very late M stars and brown dwarfs the CNS4 catalog is bound to be incomplete.

3. Data Analysis

The ROSAT source lists and the CNS4 catalog were searched for positional coincidences. As a matching criterion we used 120 arcsec for survey data, 60 arcsec for pointing data with the PSPC and 30 arcsec for HRI data. The differently chosen positional acceptance thresholds reflect the fact that, first, the intrinsic positional accuracy of survey data, and the PSPC and HRI pointing data decreases in that order, and second, the CNS4 input catalog does not have the most accurate positional information

since it is not intended to be a positional catalog. The chosen acceptance thresholds do not introduce significant errors into our X-ray source lists. In quite a few cases multiple detections of coronal X-ray emission from individual stars are available. Specifically, many of the nearby stars observed and detected made in the ROSAT pointing program were also detected in the survey data.

We stress that X-ray source identifications are made solely on the basis of positional coincidence. Nevertheless we expect the number of spurious identifications to be very small. Calculating the number of identifications obtained by distributing approximately 100 000 RASS sources over 3231 positions (i.e., the number of Gliese stars) with a detect cell radius of 2 arcmin, results in ~ 27 spurious identifications or 2% of the total number of RASS detections of nearby stars. The actual distribution of position offsets is much narrower. To be specific, only 16 out of 1217 survey detections have position offsets of more than 100 arcsec, and only 80 X-ray detections are off by more than 60 arcsec from the optical positions. We thus conclude that the fraction of incorrectly identified X-ray emitters is at the one percent level at worst.

4. The NEXXUS data base

Altogether we can associate 1333 of the 3231 stars up to a distance of 25 pc contained in the CNS4 catalog with ROSAT detected X-ray sources; the vast majority of these sources comes from the RASS data (1217). The remaining 116 stars were only detected in pointed observations. In addition to the survey detections, 328 stars were also observed with the PSPC in pointed mode without the boron filter, 49 with the filter, and 242 stars were observed with the ROSAT HRI. Moreover, some of these stars were observed more than once, so that multiple detections of coronal X-ray emission are available. For easy access and future reference the results of this cross-correlation process were assembled in the **N**earby **X**-ray and **X**UV-emitting **S**tars data base, available via www from the Home Page of the Hamburger Sternwarte at the URL <http://www.hs.uni-hamburg.de/DE/For/Gal/Xgroup/nexxus>.

For each CNS4 star detected in X-rays the database provides detailed information about the star itself, e.g. several catalog names, coordinates, proper motion, apparent and absolute magnitude, color indices, parallax and distance; and information about the associated X-ray source(s), e.g. coordinates, count rates with errors, background, exposure time, and an X-ray luminosity. For PSPC observations hardness ratios and a source likelihood are given, for HRI observations a signal to noise ratio. The date of observation, an off-axis angle, and source and sequence numbers of pointed observations are listed, too. To facilitate browsing, NEXXUS can be searched by coordinates, catalog name, color index, magnitude, proper motion or distance. For completeness we also list the XUV measurements of the CNS4 stars obtained with the ROSAT Wide Field Camera (WFC); the WFC data were kindly made available to NEXXUS

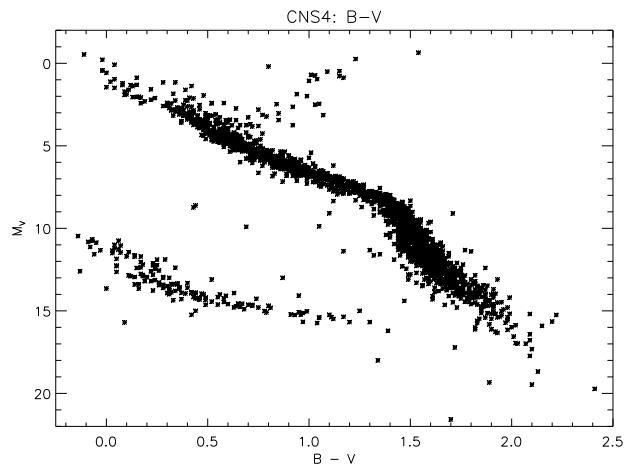


Fig. 1. Color-magnitude diagram ($B - V$ vs. M_V) for all stars contained in CNS4 catalog.

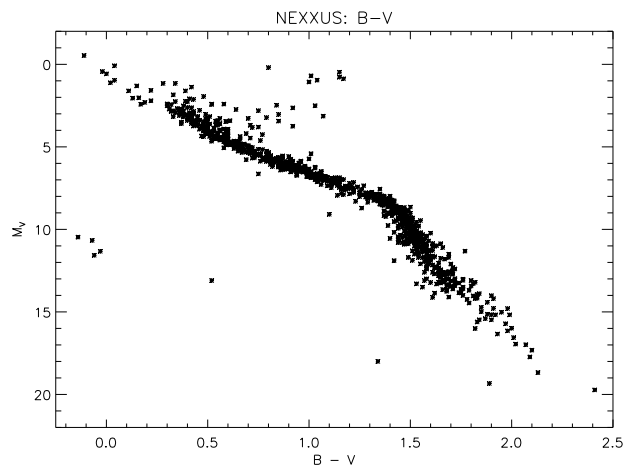


Fig. 2. Color-magnitude diagram ($B - V$ vs. M_V) for all X-ray detected stars listed in the NEXXUS data base.

by J. Pye (Leicester University). The WFC survey data is published by Pye et al. (1995), the pointed WFC-data will be discussed by Pye et al. (2003, in preparation).

5. Results

From the above cited numbers the overall ROSAT detection rate of the nearby stars listed in CNS4 is 41.1 %. It is instructive to compare a color-magnitude diagram of all CNS4 stars (cf., Fig. 1) with a similar diagram constructed only for NEXXUS stars (cf., Fig. 2). One immediately notes the well-known paucity of X-ray emitting white dwarfs as well as the absence of X-ray detected brighter giants. Stellar X-ray emission is detected down to an absolute magnitude of $M_V = 20$, i.e., down to the very bottom of the main sequence.

Except for white dwarfs and the brighter giants the overall detection rate of 41.1 % is due to the lack of sufficient sensitivity for the more distant CNS4 stars. In the following we therefore focus on the very nearest stars

for which almost complete detections are available. For this purpose we introduced three categories of stars. Since color information and spectral type are not always consistent, we decided to use a criterion based on absolute magnitudes to group our sample stars into three categories, those with M_V in the range $3 \leq M_V \leq 5.80$ i.e., the F/G-stars, those with $5.80 < M_V \leq 8.50$, i.e., the K stars, and those fainter than $M_V = 8.50$, i.e., the M-type stars. We explicitly excluded all giants or white dwarfs from these samples; specifically, the giant stars Capella (Gl 194AB), a well-known RS CVn-like binary, β Gem (= Gl 286; Hünsch et al. (1998a)) and Arcturus (= Gl 541; Ayres et al. (1991)) are not listed here. Tab. 1 contains the results for the F/G-stars, Tab. 2 those for the K stars, and Tab. 3 those for stars fainter than $M_V = 8.50$. In each table we provide the stars' names, their absolute magnitude, their spectral type and distance as listed in the CNS4 catalog provided by Jahreiss (2002). For each star we then list the measured count rate and its error, the exposure time and an X-ray luminosity. In order to convert from count rate to X-ray flux we used a conversion factor of 6×10^{-12} erg cm $^{-2}$ ct $^{-1}$ for PSPC data, 3×10^{-11} erg cm $^{-2}$ ct $^{-1}$ for PSPC with boron filter and 2.4×10^{-11} erg cm $^{-2}$ ct $^{-1}$ for HRI data; X-ray luminosities were compiled from these X-ray fluxes and the HIPPARCOS distances. For RASS and PSPC pointing data the source likelihood is given, for HRI data the signal to noise ratio of the detection. A flag indicates the source of the data; S stands for RASS data, P for PSPC pointing data without the boron filter, F for PSPC pointing data with the boron filter, and H for HRI data. If a star was observed more than once with the same instrumental setup, only the observation with the longest exposure time is listed. In the case of binaries the components are listed separately if they were resolved in any of the ROSAT observations, only one entry is given for binaries unresolved by ROSAT. As far as the X-ray data are concerned, Tab. 1-3 are meant to replace Tab. 1 in Schmitt et al. (1995) and Tab. 2 in Schmitt (1997).

5.1. Detection completeness

In Fig. 3-5 we plot for the F/G-types stars, the K-type stars and the M-type stars the X-ray luminosity (in erg/sec) as a function of distance (in pc). Inspection of Fig. 3 shows that among 69 F/G stars within a distance of 14 pc around the Sun, only seven (i.e., the stars Gl 67A, Gl 138, Gl 197, Gl 324A, Gl 354A, Gl 454 and Gl 541A) remained undetected. Note that in order to avoid multiple marks for a star observed more than once, only the observation with the longest exposure time was used to create the figures. The detection rate within the volume out to 14 pc is therefore 94 %, and all stars within 12 pc have been detected.

The K stars are plotted in Fig. 4; only two stars (i.e., Gl 776.3 and Gl 884) out of 51 have not been detected and hence the detection rate is 96 %. We remark in this con-

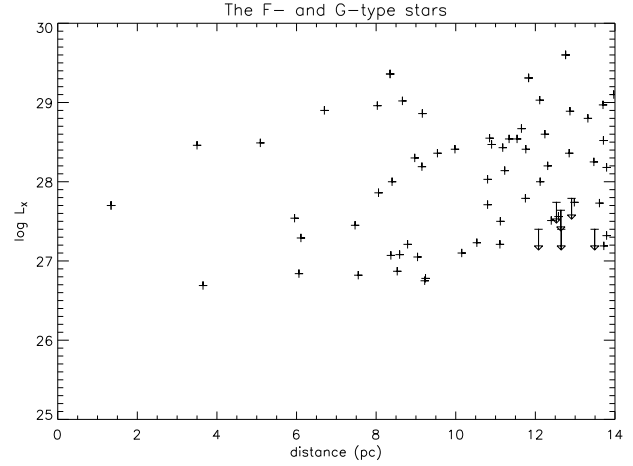


Fig. 3. L_X vs. distance for the F/G star sample; note the complete sampling out to 12 pc.

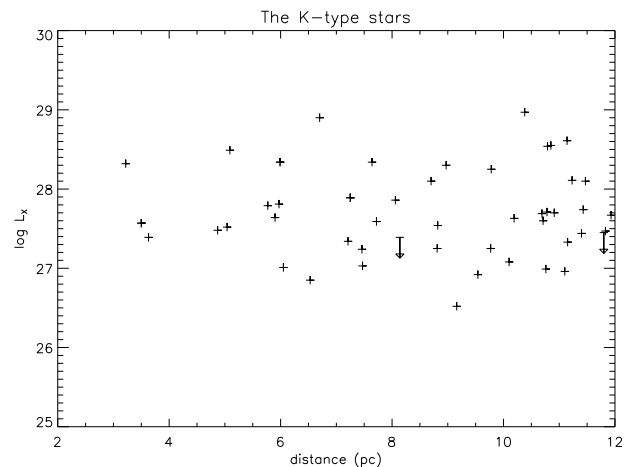


Fig. 4. L_X vs. distance for the K star sample

text that the automatic analysis failed to detect the star Gl 653 in an HRI pointing. We therefore retrieved the original X-ray data and generated an X-ray image having screened the photons to the pulse height range between channels 2-10. Inspection of this image shows a rather weak source within less than two arcsec of the expected proper motioned star position. Within a square box of 10 arcsec by 10 arcsec 12 counts were recorded with 6.1 being attributed to background; the remaining counts were then attributed to Gl 653. Obviously, a confirmation of this detection is highly desirable.

The M stars are plotted in Fig. 5; out to a distance of 6 pc 6 stars out of 65 have not been detected; the non-detected stars are Gl 570D, Gl 693, GJ 1002, LP 816-60, LP 944-20 and DENIS 1048-39. Gl 570D is a brown dwarf not detected in an HRI pointing of the Gl 570 system; LP 944-20 is another brown dwarf undetected in a series of HRI pointings (Neuhäuser et al. 1999), but with a flare detected in a *Chandra* observation (Rutledge et al. 2000). Excluding those brown dwarfs all the derived upper limits except for the star GJ 1002 are derived from survey

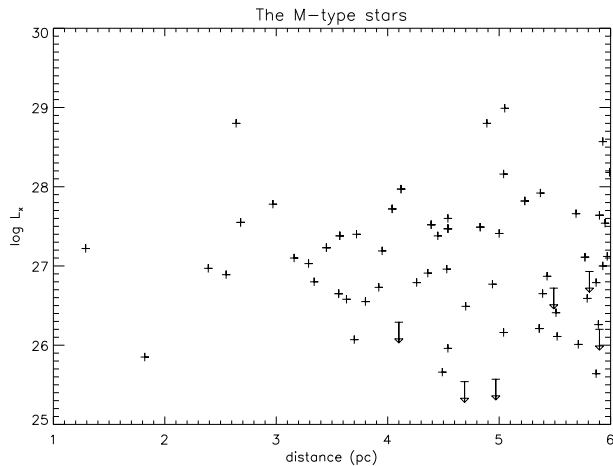


Fig. 5. L_X vs. distance for the M star sample

observations with correspondingly relatively low sensitivity. There is no reason to expect that these stars will not be detected once more sensitive X-ray observations are available. In other words, the formation of X-ray emitting coronae appears to be universal for late-type main sequence stars.

5.2. Comparison to previous work

The most complete previous compilations of X-ray data on nearby late-type stars are due to Schmitt (1994) for M and K-type stars (Table 1) and to Schmitt (1997) for F and G-type stars (Tab. 2). Compared to Tab. 1 presented by Schmitt (1997) we first note that now the HIPPARCOS distance scale has been used. As a result of this some stars previously thought to be located within 13 pc are no longer within that distance limit. Specifically, the stars Gl 55, Gl 95, Gl 97, Gl 327, Gl 364, Gl 512.1, Gl 534.1A, Gl 611A, Gl 691 and Gl 805 had to be removed from the sample. Further, the binary system Gl 107AB has been observed with the HRI and the individual components are now separated; note that Gl 107B is of type M and is not included in our nearby sample because of its distance. Also, instead of upper limits we now have detections (with the ROSAT HRI) for the G-type stars Gl 53A and Gl 442A. The M star Gl 53B has also been detected but is again not member of our nearby stellar sample because of distance, while Gl 442B (= VB 5) at a distance of 9.24 pc has not been detected in a 10 ksec ROSAT HRI pointing. Schmitt et al. (1995) had complete K star detections only out to 7 pc, now the limit is 12 pc; on the other hand, the distance limit for the M-type stars had to be reduced to 6 pc. Including the stars between 6 and 7 pc would add another 27 stars (from which, however, 7 remain undetected) and therefore significantly enlarge the number of undetected M-stars.

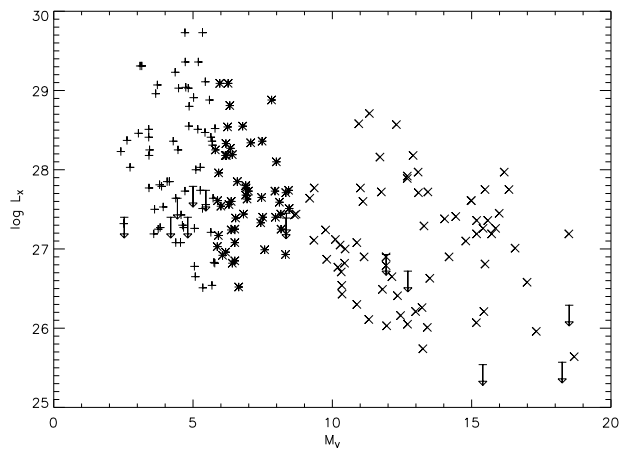


Fig. 6. X-ray luminosity vs. absolute magnitude M_V for the nearby main-sequence stars; plusses denote F/G-type stars, asterisks K-type stars and crosses M-type stars. Note the absence of solar-like stars with X-ray luminosities of 10^{26} erg/sec and below.

5.3. X-ray luminosity

In order to provide an overview over the X-ray luminosities of our sample stars we show in Fig. 6 the measured X-ray luminosity as a function of absolute magnitude M_V . Note that the **range** in X-ray luminosity for this sample is about three orders of magnitude essentially independent of spectral type, while the median X-ray luminosity is decreasing with increasing M_V . No objects are found in the right upper corner (there are no super-saturation M dwarfs) nor in the lower left corner, i.e., there are no X-ray dark solar-like stars. The dependence of median X-ray luminosity on spectral type suggests to take out the scale effect introduced by stars of different size by considering instead the mean X-ray surface flux F_X obtained by dividing L_X by the stellar surface as in Schmitt (1997).

A mean quantity such as F_X is little meaningful for “local” structures such as individual loops or active regions, however, for “global” structures such as coronal holes, it is in fact a useful and even basic quantity. The plot of F_X vs. M_V for our sample stars is shown in Fig. 7; as in Fig. 6, the three different types of symbols represent the F/G-type stars (plusses), K-type stars (asterisks) and M-type stars (crosses). Fig. 7 indicates that the mean surface flux distributions of the three classes of stars show little difference. Possibly the mean surface flux distribution of the very faintest stars is somewhat larger on average, there is some hint that for stars with $M_V < 13$ the lower envelope on F_X may actually increase. Also note that the K-star region now appears well filled, while there was a “gap” because of lacking sample size in the previously published data (cf., Fig. 8 in Schmitt (1997)). The formal cumulative distribution functions are shown in Fig. 8, showing that indeed the means and lower envelopes of the three distribution functions agree with each other with statistical accuracy. Carrying out formal testing with Smirnov

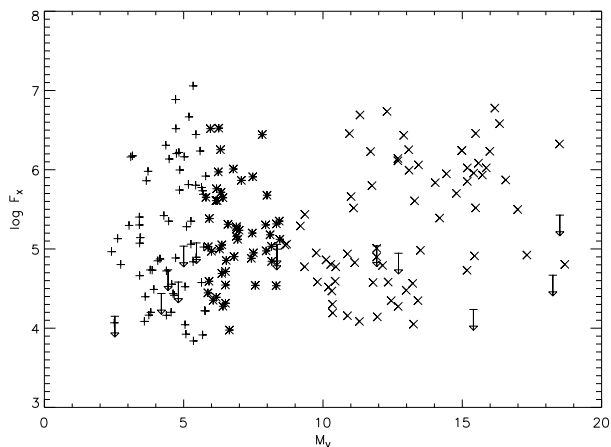


Fig. 7. Mean X-ray surface flux vs. absolute magnitude M_V for the nearby main-sequence stars; pluses denote F/G-type stars, asterisks K-type stars and crosses M-type stars. Note the lower limit of about 10^4 erg/cm²/sec of observed X-ray surface flux.

test shows that the null hypothesis that all three classes of stars are characterized by the same mean X-ray surface flux distribution function cannot be rejected and is hence consistent with the data. We therefore conclude that not only do all cool (dwarf) stars have coronae, but that also these coronae have mean X-ray fluxes of at least 10^4 erg/cm²/sec. We mention that these limits are grossly violated (a) by A-type stars, and (b) giants. For example, for Vega ($R = 2.5 R_\odot$) one would compute $L_X = 4 \times 10^{27}$ erg/sec; interpreting the upper limit of $1.2 \cdot 10^{-3}$ cts/sec, that Schmitt (1997) attributes to UV contamination, as X-ray flux, one obtains $L_X \sim 5.5 \cdot 10^{25}$ erg/sec, i.e., two orders of magnitude lower than “expected”, and for Arcturus ($R = 25 R_\odot$) one obtains $L_X \sim 4 \times 10^{29}$ erg/sec, four orders of magnitude higher than the observed upper limit of $3 \cdot 10^{25}$ erg/sec (Ayres et al. 1991). The physics of coronal formation in those stars must be very different and in all likelihood those two stars are devoid of any corona.

5.4. Time variability

5.4.1. Variability between survey and pointing data

For a rather large sample of stars multiple X-ray detections are available from the RASS data and the ROSAT PSPC pointing program, which are all listed in the NEXXUS data base. In Fig. 9 we plot the PSPC count rate observed during the all-sky survey vs. the PSPC count rate observed during the pointing program in a double-logarithmic representation for those of our sample stars detected in both observing modes; the two long-dashed lines delineate a factor of two deviation above and below unity. As is obvious from Fig. 9, except for four stars, all measurements lie within those dashed lines. The time span between survey and pointed observations varies considerably from star to star, but is typically of the order

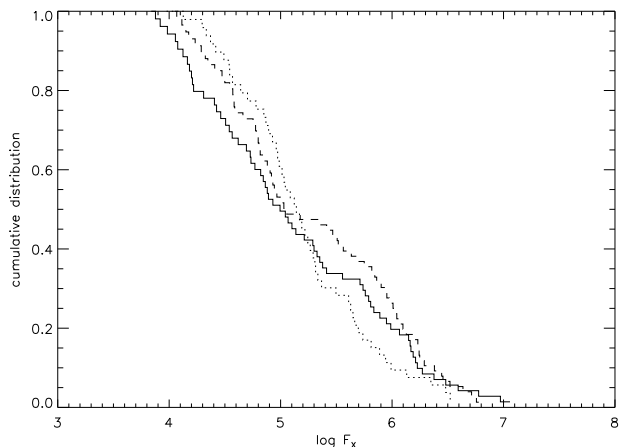


Fig. 8. Cumulative distribution function of the mean X-ray surface fluxes for F/G-type stars (stepped curve), K-type stars (dotted stepped curve) and M-type stars (dashed stepped curve). Note the close resemblance of the curves with indistinguishable mean and minimum.

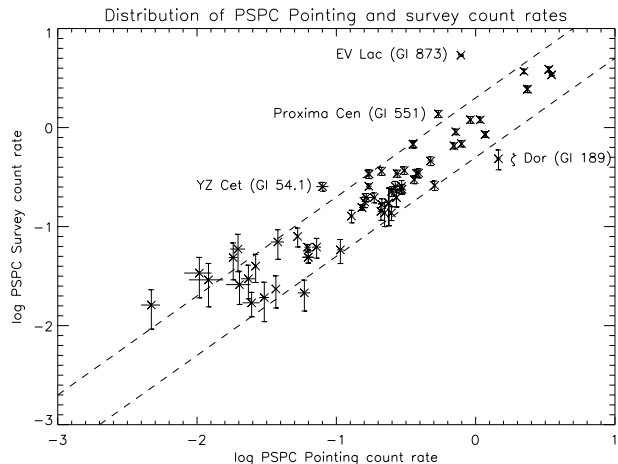


Fig. 9. Comparison of X-ray count rates for sample stars detected both in the all-sky survey and the PSPC pointing program; dashed lines indicate a factor 2 variation from unity and stars with large deviations from regression line are identified.

of 1-2 years. Obviously, variations by more than a factor of 4 are unusual at least on that time scale. The stars EV Lac, Proxima Cen and YZ Cet, all of which are well known flare stars, have significantly larger survey count rates. In the case of EV Lac this is due to a major flare which occurred during the survey observations (Schmitt 1994), the RASS light curve of Proxima Cen is discussed by Fleming et al. (1993), the RASS data on YZ Cet is discussed by Tsikoudi et al. (2000). In the case of ζ Dor (spectral type F7) the count rate observed in the pointing program was significantly higher than during the survey observations; this applies to both the PSPC observations with and without filter which had been executed immediately after each other.

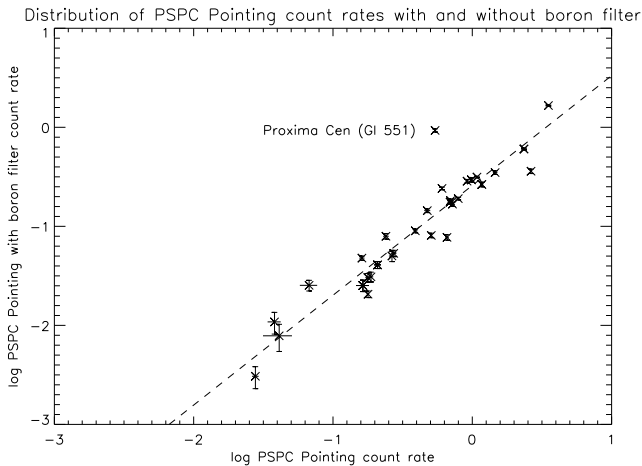


Fig. 10. Comparison of X-ray count rates for all NEXXUS stars detected in the PSPC pointing program with and without boron filter; stars with large deviations from regression line are identified.

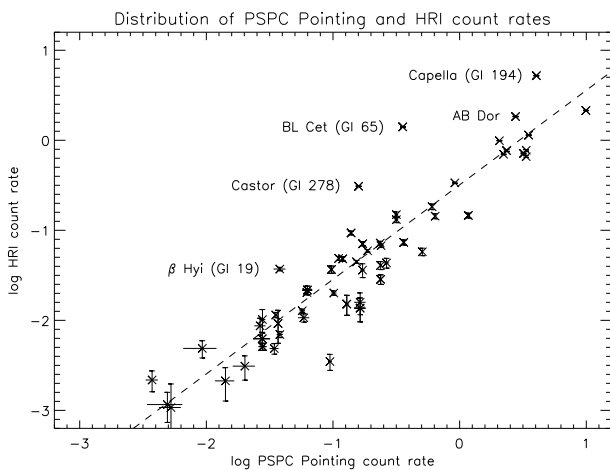


Fig. 11. Comparison of X-ray count rates for all NEXXUS stars detected both in the PSPC and HRI pointing program; stars with large deviations from regression line are identified.

In Fig. 10 we plot the PSPC pointing mode count rates measured with and without the boron filter for those NEXXUS stars observed with these instrumental setups. Observations with this setup were typically (albeit not always) taken immediately adjacent to each other, so that the time span between the data sets for a given stars should usually be of the order of a few hours. Of course, the spectral response of the PSPC detector with and without the boron filter differs especially at soft X-ray energies below the carbon edge, yet, one observes a well defined regression curve extending over two orders of magnitude. The only star far away from the regression line is again the well known flare star Proxima Cen, which clearly flared during the boron filter observation.

In Fig. 11 we plot the PSPC count rate measured in pointing program data vs. the HRI count rate in a double-

logarithmic representation for those of the NEXXUS stars detected in both observing modes. In contrast to the boron filter data, the time span between PSPC and HRI pointed observations is much longer and is typically of the order of a few years for most stars. Also note that the spectral response of the HRI differs somewhat from that of the PSPC. Again, we see a good correlation between PSPC and HRI count rates over two orders of magnitude with a larger dispersion than observed for the comparison between boron and open PSPC data, but with similar dispersion as observed for the pointed and survey PSPC data for the same stars. Again, for multiply observed stars only the observation with the longest exposure time was taken into account to compile Fig. 10 and 11.

5.4.2. Variability of individual stars

For a small number of stars repeated observations were carried out with the same instrumental setup. These datasets are discussed for the individual sources in the following section.

α Cen A/B: The α Cen A/B system was observed twice with the ROSAT HRI for an extended period of time. The first set of observations was carried out in February 1996, the second one in August 1996. The obtained ROSAT HRI light curves for α Cen A/B are shown in Fig. 12 and 13. In both light curves the stars denote the measurements of α Cen B, the crosses those of α Cen A. As is apparent from Fig. 12 and 13, the B component is brighter than the A component at least every time the system was looked at with the HRI. α Cen A shows small daily variations, the overall level of X-ray emission was slightly higher during the August observations. α Cen B showed considerably more X-ray variability than the A component. In February 1996 the overall emission level was higher, an excursion to more than 1 HRI cts/sec was observed on day. During the second observation in August 1996 the count rate decreased by about 30 percent over a 20 day interval, afterwards the count rate started increasing again. We interpret the high count rate episode in α Cen B as a flare, the 20 day decrease in count rate might be due to rotational modulation. NEXXUS lists two PSPC pointings on α Cen A/B, one in September 1992 for 3260 seconds and one in September 1993 for 357 seconds. During the September 1993 pointing the count rate was more than twice the count rate observed during the September 1992 and the RASS observations and the hardness ratio was significantly enhanced. An inspection of arrival positions of the individual photons suggests the K star as the source of the increased X-ray radiation in line with the light curve Fig. 12. We therefore conclude that α Cen B is a flare star.

Gl 86: The star Gl 86 was serendipitously observed during a monitoring campaign on the blazar PKS 0208-512 with the ROSAT PSPC. 12 pointings almost more or less equally spaced in time were carried out over a 13 day interval. The resulting ROSAT PSPC light curve for

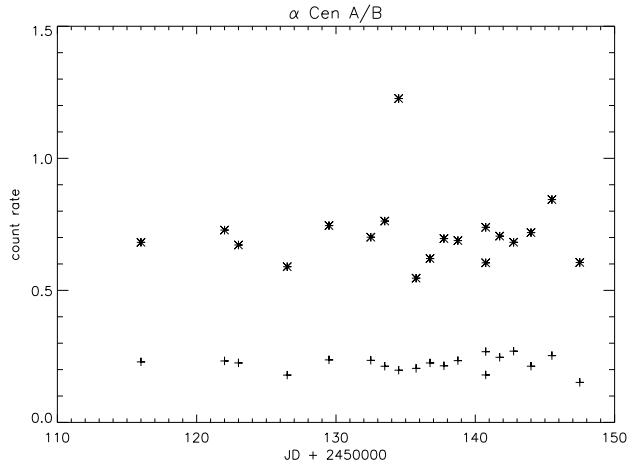


Fig. 12. X-ray light curve for α Cen A/B (Gl 559AB) in February 1996; asterisks denote measurements for α Cen B, plusses measurements for α Cen A.

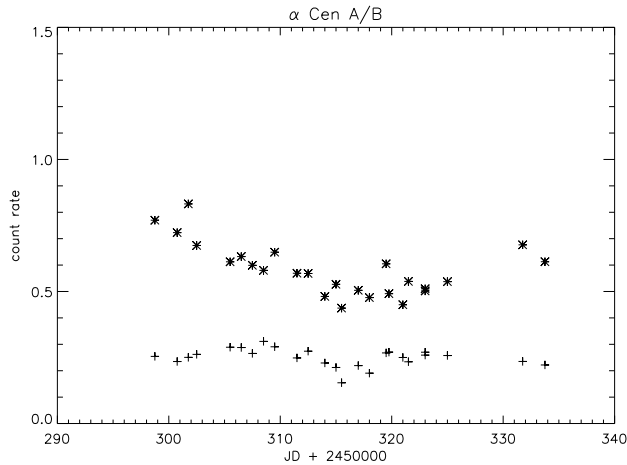


Fig. 13. X-ray light curve for α Cen A/B (Gl 559AB) in August 1996; asterisks denote measurements for α Cen B, plusses measurements for α Cen A.

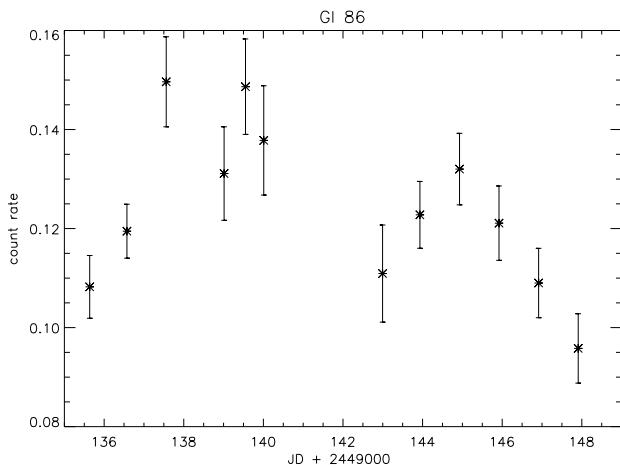


Fig. 14. X-ray light curve for Gl 86 in May/June 1993

Gl 86 is shown in Fig. 14. The count rate first increased by almost a factor of 1.5 during the first half of the observations. After a 3-day gap the count rate started to increase in the second half again from the level it started in the first half, and then it decreased below that level. Variations in the X-ray output of Gl 86 are quite apparent; interestingly, Marino et al. (2002) do not find variability in Gl 86 at a confidence level higher than 90 % on short time scales.

Gl 820 A/B: The visual binary 61 Cyg A and B was angularly resolved and extensively observed with the ROSAT HRI to monitor the long-term X-ray light curve of the two stars. Since these stars were also simultaneously observed in Ca H and K, these synoptic data is presented separately by Hempelmann et al. (2003, in preparation).

LHS 288: A special note is appropriate for the star LHS 288. Schmitt et al. (1995) report an upper limit of < 0.01 cts/sec at the position of LHS 288 from the ROSAT all-sky survey data, while Marino et al. (2000) report a detection of LHS 288 from a PSPC pointed observation. The count rate level of 0.19 cts/sec reported by Marino et al. (2000) would have been easily detectable in the RASS data, however, the position of the X-ray source reported by Marino et al. (2000) does not agree with expected optical position of LHS 288 in CNS4 or in Luyten's catalog. Investigating this discrepancy we realized that Bakos et al. (2002) were unable to find and confirm even the existence of LHS 288 in their systematic attempt to follow-up high proper motion stars listed in the LHS catalog. We therefore decided to investigate the DSS images in the R and V bands in the vicinity of the expected position of LHS 288. We compared the DSS images taken at epochs 1987.0512 and 1991.1096, searched for moving objects and found evidence only for one object with significant proper motion, which turned out to be also very red. The 1987.0512 position of this object is R.A. 10:44:22.11, δ -61:12:55.2 (w.r.t. equinox 2000). The position of the X-ray source reported by Marino et al. (2002) is R.A. 10:44:21.9 and δ -61:12:44 at epoch 1993.5575 (w.r.t. equinox 2000). According to CNS4, the proper motion of LHS 288 is 1.66 arcsec/year almost due north. Applying the proper motion of LHS 288 as listed in CNS4 to the position derived for the red moving DSS object results in almost perfect agreement with the PSPC X-ray position. We therefore conclude that the red moving DSS object is the X-ray source reported by Marino et al. (2000), and that this object is identical with LHS 288. Thus, LHS 288 has been re-found and does exist. We emphasize that also at the new position no X-ray source can be found in the RASS data with an upper limit of < 0.03 cts/sec.

In August 1996 a 12927 sec pointed observation was carried out on LHS 288 with the ROSAT HRI. Although the automatic analysis did not show any X-ray source at the correct position of LHS 288 and consequently an appropriate entry in the ROSAT source catalogs is missing, a visual inspection of the ROSAT HRI image and a re-analysis of the individual X-ray photons revealed the presence of a weak, but still significant source at the position R.A. 10:44:20.99, δ -61:12:38.3 in perfect agreement

with the previously derived (and proper-motioned) PSPC and DSS positions. The observed count rate of LHS 288 as observed in August 1996 was $\approx 7.9 \cdot 10^{-4}$ HRI cts/sec; applying a factor of 4 to convert to an equivalent PSPC count rate (cf., Fig. 11), we find an equivalent PSPC rate of $\approx 3.2 \cdot 10^{-3}$ PSPC cts/sec, which is clearly consistent with the survey non-detection of LHS 288, but not with the detection of LHS 288 in the pointing program. We thus conclude that during the short PSPC pointing on July 21, 1993 the X-ray flux of LHS 288 was almost two orders magnitude larger than during the RASS observations and during the HRI pointing in August 1996, and that the PSPC observations on July 21, 1993 caught LHS 288 in an unusual state.

6. Conclusions

This paper attempts to provide a final and hopefully definitive summary of the ROSAT observations of nearby stars. It extends our previous studies of the subject and the now presented source tables supersede those published previously. One of our main results is the universality of X-ray emission among late-type stars with outer convection zones. As to the F/G-type stars, all stars at distances below 12 pc have been detected, all the upper limits obtained in the distance range 12 - 14 pc result from the lower sensitivity survey data. As to the K-type stars, all stars at distances below 8 pc have been detected and only two stars in the distance range 8 - 12 pc remain undetected; two of those upper limits come from survey data, the other one is derived from a rather short ROSAT HRI pointing. As to the M-type stars, only two stars in the volume out to 6 pc remain undetected if very late-type stars and brown dwarfs are excluded from consideration; one upper limit comes from survey data, one from a short PSPC pointing. If all known stars within 6 pc are included, the number of non-detected stars increases to 6; in one case (LP 944-20) a Chandra detection of such an object during a flare has been obtained. We therefore conclude that all main-sequence stars with outer convection zones are surrounded by hot coronae and that the reason for our not being able to detect all stars is lack of sufficient sensitivity rather than the intrinsic absence of X-ray emission. X-ray dark cool stars on the main sequence do not exist.

The X-ray luminosities of cool dwarf stars extend over three orders of magnitude with the mean values decreasing with decreasing spectral type. Scaling the X-ray luminosity with the stellar surface results in an activity measure F_X independent of spectral type with essentially indistinguishable distribution functions. In particular, stars with the lowest degree of activity in any subclass always have mean X-ray surface fluxes of $\approx 10^4$ erg/cm²/sec. Schmitt (1997) demonstrated that this flux level is approximately the one attained by solar coronal holes, the much larger sample available now confirms this conclusion. Of course, there is no direct proof that the X-ray emission originates from magnetically open (rather than closed) regions in those stars. However, the fact that the lower surface flux

level is so similar from F-type stars through to M-type stars as well as the lack of observed variability suggest a global rather than a local property as cause of the observed similarities. As an interesting aside we note that for a star like the Sun the X-ray luminosity contained in this ‘‘coronal hole’’-component amounts to approximately 6×10^{26} erg/sec formally in the 0.1 - 2 keV, with actually almost all flux contained in the 0.1 - 0.5 keV band because of the low X-ray temperatures (cf., Fig. 7 in Schmitt (1997)). Relating this value to the bolometric luminosity via $L_{X,CH}/L_{bol}$ results in a value of approximately 1.5×10^{-7} , i.e., the same value found to describe the X-ray emission from early type stars (which is also thought to arise in winds). It is unclear whether this agreement is simply a numerical coincidence or indicative of a physical connection.

The question of X-ray emission among the very latest main-sequence stars and brown dwarfs remains unclear. ROSAT observations usually do not have the sensitivity level to reach the required surface flux levels of 10^4 erg/cm²sec at the stellar surface; for a typical star at the bottom of the main sequence this corresponds to an X-ray luminosity of 6×10^{24} erg/sec (in the 0.1 - 0.5 keV band) which is hard to detect even for stars in the immediate solar vicinity. More importantly, the observed large amplitudes of X-ray variability as seen for vB10 (=G1 752B; Fleming et al. (2000)), LHS 2065 ((Schmitt & Liefke 2002)), LP 944-20 (Rutledge et al. 2000) and for LHS 288 (this paper) suggest that the physics of coronal formation for very low mass stars and brown dwarfs may be different and X-ray emission may be present only in a transient fashion.

This behavior with large amplitude variability has to be juxtaposed to the the relatively small degree of X-ray variability found for stars of low activity levels in extensive ROSAT observations. Comparison of stars with multiple PSPC observations (in particular for stars with both survey and pointing detections available) shows that for most stars the two data sets are within a factor of two from unity; the only stars with discrepant fluxes are known flare stars, where the observed count rate excursions can be clearly attributed to flare events. The Sun is known to vary its X-ray output during a solar cycle by almost two orders of magnitude (Acton 1996), however, the observed amplitude of variability strongly depends on the spectral band considered. The YOHKOH data described by (Acton 1996) refer to a somewhat harder X-ray band than the typical ROSAT data are referred to, and therefore a solar peak-to-peak variation in the ROSAT band of a factor 100 during a solar cycle seems too extravagant an expectation. At any rate, from the ROSAT observations we can state that count rate variations usually stay within a factor of 4 with exceptions attributable to flares. So, either the stellar variability level is lower or the time full time scale of variability has not been adequately sampled by ROSAT.

Acknowledgements. The ROSAT work on nearby stars would have been impossible without the ROSAT all-sky survey. We thank H. Jahreiss for making available to us his latest version of CNS4. We have made extensive use of the ROSAT Data Archive of the Max-Planck-Institut für extraterrestrische Physik (MPE) at Garching, Germany. Also, this research has made use of the SIMBAD database, operated at CDS, Strasbourg, France. We particularly thank Dr. J. Pye for providing us with the ROSAT-WFC data for inclusion into the NEXXUS data base. We thank our many colleagues for numerous discussions on the X-ray properties of nearby stars.

References

- Acton, L. 1996, in ASP Conf. Ser. 109: Cool Stars, Stellar Systems, and the Sun, 45–55
- Ayres, T. R., Fleming, T. A., & Schmitt, J. H. M. M. 1991, *ApJ*, 376, L45
- Bakos, G. Á., Sahu, K. C., & Németh, P. 2002, *ApJS*, 141, 187
- Berghöfer, T. W., Schmitt, J. H. M. M., Danner, R., & Cassinelli, J. P. 1997, *A&A*, 322, 167
- Delfosse, X., Forveille, T., Martín, E. L., et al. 2001, *A&A*, 366, L13
- Fleming, T. A., Giampapa, M. S., & Schmitt, J. H. M. M. 2000, *ApJ*, 533, 372
- Fleming, T. A., Giampapa, M. S., Schmitt, J. H. M. M., & Bookbinder, J. A. 1993, *ApJ*, 410, 387
- Fleming, T. A., Snowden, S. L., Pfeffermann, E., Briel, U., & Greiner, J. 1996, *A&A*, 316, 147
- Fuhrmeister, B. & Schmitt, J. H. M. M. 2003, *A&A*, in press,
- Hünsch, M. 2001, in ASP Conf. Ser. 223: 11th Cambridge Workshop on Cool Stars, Stellar Systems and the Sun, 967–971
- Hünsch, M., Schmitt, J. H. M. M., Sterzik, M. F., & Voges, W. 1999, *A&AS*, 135, 319
- Haisch, B. & Schmitt, J. H. M. M. 1994, *ApJ*, 426, 716
- Hünsch, M., Schmitt, J. H. M. M., & Voges, W. 1998a, *A&AS*, 127, 251
- Hünsch, M., Schmitt, J. H. M. M., & Voges, W. 1998b, *A&AS*, 132, 155
- Jahreiss, H. 2002, private communication
- Marino, A., Micela, G., & Peres, G. 2000, *A&A*, 353, 177
- Marino, A., Micela, G., Peres, G., & Sciortino, S. 2002, *A&A*, 383, 210
- Neuhäuser, R., Briceño, C., Comerón, F., et al. 1999, *A&A*, 343, 883
- Pye, J. P., McGale, P. A., Allan, D. J., et al. 1995, *MNRAS*, 274, 1165
- Randich, S. 2000, in ASP Conf. Ser. 198: Stellar Clusters and Associations: Convection, Rotation, and Dynamics, 401–
- Rutledge, R. E., Basri, G., Martín, E. L., & Bildsten, L. 2000, *ApJ*, 538, L141
- Schmitt, J. H. M. M. 1994, *ApJS*, 90, 735
- Schmitt, J. H. M. M. 1997, *A&A*, 318, 215
- Schmitt, J. H. M. M., Fleming, T. A., & Giampapa, M. S. 1995, *ApJ*, 450, 392
- Schmitt, J. H. M. M., Golub, L., Harnden, F. R., et al. 1985, *ApJ*, 290, 307
- Schmitt, J. H. M. M., Kahabka, P., Stauffer, J., & PETERS, A. J. M. 1993, *A&A*, 277, 114
- Schmitt, J. H. M. M. & Liefke, C. 2002, *A&A*, 382, L9
- Scholz, R.-D., Meusinger, H., & Jahreiß, H. 2001, *A&A*, 374, L12
- Schröder, K.-P., Hünsch, M., & Schmitt, J. H. M. M. 1998, *A&A*, 335, 591
- Simon, T., Drake, S. A., & Kim, P. D. 1995, *PASP*, 107, 1034
- Stern, R. A., Schmitt, J. H. M. M., & Kahabka, P. T. 1995, *ApJ*, 448, 683
- Sterzik, M. F. & Schmitt, J. H. M. M. 1997, *AJ*, 114, 1673
- Tsikoudi, V., Kellett, B. J., & Schmitt, J. H. M. M. 2000, *MNRAS*, 319, 1136
- Vaiana, G. S., Fabbiano, G., Giacconi, R., et al. 1981, *ApJ*, 245, 163

Table 1: Sample stars with absolute magnitude between 3.00 and 5.80 (and some F-type stars brighter than 3.00) and a distance up to 14 pc, the F- and G-type stars. Table contains the star’s name (col 1), its absolute visual magnitude (col 2), and its spectral type (col 3) as in CNS4; the distance (in pc, col 4) is computed from the CNS4 parallax. Mode (col 5) denotes the source of the X-ray data, S denoting survey data, P pointed PSPC data, and H pointed HRI data. The countrate (col 6) and its error (col 7) are quoted in cts/sec, the likelihood or SNR are dimensionless (col 8), the exposure time (col 9) is in seconds, and the X-ray luminosity (col 10) in cgs-units.

Catalogue Name	M_V	Spectral Type	Distance (pc)	Mode	Count Rate	Error	Likelihood or S/N	Exposure Time	$\log L_x$
G1 5	5.44	K0 V e	13.70	S	0.686800	0.048430	624.0	327	28.97
				P	0.793700	0.017800	3690.0	2575	29.03
				F	0.190600	0.005840	8385.0	5806	29.11
G1 17	4.55	F9 V	8.59	P	0.022820	0.003500	75.0	2385	27.08
G1 19	3.42	G2 IV	7.47	S	0.069990	0.023200	15.0	195	27.45
				P	0.038040	0.004100	114.0	2668	27.18
				F	0.010850	0.002680	26.0	1667	27.34
G1 27	5.64	K0 V	11.11	H	0.037140	0.001630	21.0	14526	27.77
				H	0.004537	0.000952	4.9	6405	27.21
				S	0.137900	0.021990	71.0	381	27.54
G1 34A	4.57	G3 V	5.95	H	0.026470	0.002070	10.2	6391	27.43
G1 53A	5.78	G5 VI	7.55	H	0.004004	0.000662	6.0	12750	26.82
G1 61	3.44	F8 V	13.47	S	0.134900	0.022790	66.0	354	28.25
G1 67A	4.44	G1.5 V	12.64	S	<0.03801		2.1	377	27.64
G1 71	5.68	G8 Vp	3.65	S	0.051750	0.013440	24.0	445	26.69
				H	0.009015	0.002360	3.9	2000	26.54
G1 75	5.64	K0 V	9.98	S	0.360200	0.026490	505.0	572	28.41
G1 92A	4.85	G0 V e	10.85	S	0.423400	0.039160	285.0	299	28.55
G1 107A	3.87	F7 V	11.23	S	0.152400	0.018690	140.0	527	28.14
				H	0.016830	0.002590	5.5	2850	27.79
G1 111	3.72	F6 V	13.97	S	0.906300	0.059260	559.0	288	29.10
				P	0.721600	0.020700	3473.0	1779	29.00
				F	0.167500	0.008840	4878.0	2136	29.07
G1 124	3.93	G0 V	10.53	S	0.021440	0.007394	13.0	523	27.23
				P	0.058940	0.006000	145.0	1821	27.67
				H	0.010690	0.001140	8.8	9309	27.53
G1 136	5.10	G2 V	12.12	S	0.095070	0.020590	35.0	328	28.00
G1 137	5.02	G5 V e	9.16	S	1.201000	0.094630	472.0	286	28.86
				P	0.917700	0.024400	3994.0	1594	28.74
				F	0.285900	0.011600	4366.0	2144	28.94
				H	0.336300	0.005450	52.8	11246	28.91
G1 138	4.81	G1 V	12.08	S	<0.02417		0.5	338	27.40
G1 139	5.35	G5 V	6.06	S	0.025950	0.009569	10.0	519	26.84
				P	0.020170	0.004010	39.0	1738	26.73
				H	0.003099	0.000932	3.6	5913	26.51
G1 147	3.59	F8 V	13.72	P	0.011510	0.002340	15.0	2809	27.19
G1 150	3.75	K0 IVe	9.04	S	0.019220	0.008239	9.0	532	27.05
				P	0.030400	0.002490	178.0	6383	27.25
G1 177	4.86	G1 V	13.32	S	0.490200	0.045960	272.0	539	28.80
G1 178	3.66	F6 V	8.03	S	1.957000	0.146700	481.0	392	28.96
G1 189	4.36	F7 V	11.65	S	0.484500	0.109600	26.0	1236	28.67
				P	1.459000	0.053800	4208.0	500	29.15
				F	0.349300	0.015200	3505.0	1507	29.23
G1 197	4.20	G2 IV-V	12.65	S	<0.02212		4.2	456	27.40
G1 211	5.79	K1 V e	12.24	S	0.368900	0.032980	331.0	367	28.60
				P	0.307700	0.007600	4435.0	5498	28.52
G1 216A	3.82	F6 V	8.97	S	0.343000	0.028840	330.0	488	28.30
				P	0.032120	0.004440	64.0	2016	27.27
G1 222AB	4.74	G0 V	8.66	S	1.942000	0.068150	2940.0	431	29.02
				F	0.408600	0.008850	9999.0	5284	29.04
				H	0.426400	0.011600	31.9	3119	28.96
G1 231	5.05	G5 V	10.15	S	0.017000	0.004695	21.0	1166	27.10
				P	0.024660	0.003440	50.0	2660	27.26
G1 280A	2.63	F5 IV-V	3.50	S	3.655000	0.097970	5080.0	400	28.51

Table 1: Continued

Catalogue Name	M_V	Spectral Type	Distance (pc)	Mode	Count Rate	Error	Likelihood or S/N	Exposure Time	$\log L_x$
				P	2.641000	0.027000	9999.0	3654	28.37
				F	0.360200	0.018800	3793.0	1061	28.20
Gl 302	5.45	G7.5 V	12.58	S	0.032240	0.011320	13.0	355	27.56
Gl 324A	5.46	G8 V	12.53	S	<0.04913		3.6	337	27.74
Gl 354A	2.53	F6 IV	13.49	S	<0.01938		2.1	397	27.40
Gl 356A	5.17	G8 V	11.18	S	0.298200	0.026960	254.0	467	28.43
				P	0.362400		779.0	3899	28.51
				H	0.073430	0.004580	11.0	3526	28.42
Gl 395	4.29	F8 V	12.85	S	0.195400	0.020980	172.0	572	28.36
Gl 423AB	4.72	G0 V e	8.35	S	4.539000	0.157500	3380.0	192	29.36
Gl 434	5.43	G8 V e	9.54	S	0.348000	0.037120	194.0	314	28.36
				P	0.390100	0.014200	3272.0	1956	28.41
				F	0.090090	0.004100	3880.0	5572	28.47
Gl 442A	5.05	G5 V	9.24	H	0.002430	0.000621	3.6	10109	26.78
Gl 449	3.41	F9 V	10.90	S	0.343700	0.030270	264.0	417	28.47
				P	0.377500	0.007230	4123.0	7433	28.51
Gl 454	5.00	K0 IV	12.91	S	<0.05198		7.9	352	27.79
Gl 475	4.66	G0 V	8.37	S	0.023470	0.008381	12.0	509	27.07
				P	0.036830		148.0	20537	27.27
Gl 482AB	3.10	F0 V	11.83	S	2.039000	0.121100	888.0	146	29.31
Gl 502	4.46	G0 V	9.15	S	0.255000	0.037070	78.0	504	28.19
				P	0.294400	0.006210	3909.0	8010	28.25
Gl 506	5.08	G6 V	8.53	P	0.014160	0.002460	50.0	3113	26.87
				H	0.002125	0.000856	2.8	5419	26.65
Gl 534	2.41	G0 IV	11.34	S	0.143800	0.023100	55.0	377	28.12
				P	0.185100	0.005610	1770.0	6404	28.23
Gl 559A	4.38	G2 V	1.34	S	3.876000	0.211800	589.0	420	27.70
				P	3.357000	0.033600	9999.0	3260	27.64
				H	0.658200	0.014700	25.0	3038	27.53
Gl 559B	5.72	K0 V	1.34	S	3.876000	0.211800	589.0	420	27.70
				P	3.357000	0.033600	9999.0	3260	27.64
				H	0.773600	0.015900	48.9	3038	27.60
Gl 566A	5.59	G8 V e	6.70	S	2.440000	0.183400	416.0	400	28.90
				P	2.351000	0.020700	9999.0	5213	28.88
				F	0.604100	0.011900	9999.0	4270	28.99
				H	0.767300	0.017400	32.7	2495	29.00
Gl 567	5.70	K2 V	11.54	S	0.362900	0.034130	245.0	398	28.54
				P	0.211600		1735.0	13998	28.31
Gl 575A	4.71	F9 V n	12.76	S	3.414000	0.076010	9070.0	612	29.60
				P	3.510000	0.040400	9999.0	2166	29.61
				H	1.141000	0.005250	190.6	40853	29.73
Gl 575B	5.34	dG2	12.76	S	3.414000	0.076010	9070.0	612	29.60
				P	3.510000	0.040400	9999.0	2166	29.61
				H	1.141000	0.005250	190.6	40853	29.73
Gl 598	4.07	G0 V	11.75	S	0.062080	0.014010	30.0	503	27.79
				P	0.072190	0.005470	251.0	2726	27.85
Gl 601A	2.40	F2 IV	12.31	S	0.144300	0.024700	58.0	365	28.20
Gl 603	3.62	F6 V	11.12	S	0.035450	0.011590	10.0	560	27.50
Gl 620.1A	4.83	G3/5 V	12.87	S	0.654400	0.044910	646.0	349	28.89
				P	0.699200	0.020600	3231.0	1724	28.92
				F	0.181900	0.007560	4302.0	3269	29.03
Gl 624	4.48	G0 V	12.11	S	1.027000	0.080740	493.0	166	29.03
Gl 635AB	2.74	G0 IV	10.80	S	0.127800	0.018560	77.0	494	28.03
				P	0.128600	0.004240	2371.0	7752	28.03
				H	0.015160	0.003790	3.9	1219	27.71
Gl 666A	5.75	G8 V	8.79	S	0.029000	0.013510	8.0	251	27.21
				P	0.012090	0.003340	10.0	1250	26.83
Gl 695Aa	3.80	G5 IV	8.40	S	0.197000	0.018860	232.0	718	28.00
				P	0.163900	0.017000	95.0	587	27.92

Table 1: Continued

Catalogue Name	M_V	Spectral Type	Distance (pc)	Mode	Count Rate	Error	Likelihood or S/N	Exposure Time	$\log L_x$
				F	0.025270	0.003300	98.0	2473	27.81
				H	0.015870	0.004320	3.6	910	27.51
Gl 702A	5.68	K0 V e	5.09	S	1.649000	0.127200	410.0	347	28.49
				F	0.247300	0.011500	4242.0	1903	28.36
				H	0.210900	0.016400	11.0	778	28.20
Gl 713A	4.15	F7 V	8.06	S	0.155800	0.009018	506.0	2629	27.86
				P	0.152800	0.006840	2255.0	3490	27.85
Gl 722	5.26	G5 V	12.98	S	0.045080	0.016000	15.0	283	27.74
Gl 771A	3.04	G8 IV	13.71	S	0.247900	0.029290	202.0	343	28.52
				H	0.052870	0.006060	7.6	1474	28.46
Gl 780	4.62	G8 V	6.11	S	0.073070	0.027780	10.0	124	27.29
				H	0.018620	0.002170	8.2	4350	27.30
Gl 827	4.38	F8 V	9.22	P	0.009295	0.002730	22.0	1820	26.75
				H	0.004878	0.001060	4.9	5914	27.08
Gl 848AB	3.41	F5 V	11.76	S	0.259900	0.024040	261.0	505	28.41
Gl 853A	4.71	G1 V	13.61	S	0.040330	0.013370	12.0	359	27.73
Gl 903	2.51	K1 IVe	13.79	S	0.014180	0.004882	12.0	977	27.29
				P	0.015300	0.001930	110.0	5669	27.32
Gl 904	3.42	F7 V	13.79	S	0.111500	0.019300	73.0	373	28.18
Gl 914A	5.34	G3 V	12.40	S	0.029120	0.011240	12.0	369	27.51

Table 2: Sample stars with absolute magnitude between 5.80 and 8.50 and a distance up to 12 pc, the K-type stars; columns as in Tab. 1.

Catalogue Name	M_V	Spectral Type	Distance (pc)	Mode	Count Rate	Error	Likelihood or S/N	Exposure Time	$\log L_x$
Gl 33	6.37	K2 V	7.46	S	0.043170	0.013090	17.0	353	27.24
Gl 66AB	6.26	K2 V	8.15	S	0.260478	0.039944	99.0	189	29.09
Gl 68	5.87	K1 V	7.47	P	0.026610	0.002680	135.0	4076	27.03
				H	0.008686	0.001860	4.4	3055	27.14
Gl 86	5.92	K0 V	10.91	S	0.058230	0.015840	24.0	375	27.70
				P	0.106900	0.005600	1046.0	3587	27.96
Gl 92B	6.78		10.85	S	0.423400	0.039160	285.0	299	28.55
Gl 105A	6.53	K3 V	7.21	S	0.058490	0.019040	19.0	232	27.34
				H	0.016400	0.000909	16.4	21213	27.39
Gl 117	5.96	K2 V	10.38	S	1.200000	0.077170	883.0	220	28.97
				P	1.081000	0.016700	9999.0	3880	28.92
				F	0.314700	0.006020	9999.0	8609	29.09
Gl 144	6.18	K2 V	3.22	S	2.822000	0.233500	327.0	374	28.32
				F	0.532700	0.013400	9999.0	3045	28.30
				H	0.712300	0.012400	51.8	4585	28.33
Gl 166A	5.91	K1 V e	5.04	S	0.179500	0.024990	93.0	341	27.52
				H	0.020360	0.004740	4.2	1022	27.17
Gl 169	7.99	K7 V	11.47	S	0.133200	0.019570	116.0	429	28.10
Gl 183	6.50	K3 V	8.81	S	0.032200	0.012500	9.0	387	27.25
Gl 216B	6.41	K2 V	8.97	S	0.343000	0.028840	330.0	488	28.30
				P	0.273300	0.011900	2705.0	2013	28.20
				F	0.053350	0.003930	2350.0	3540	28.19
Gl 250A	6.89	K3 V	8.70	S	0.229300	0.031610	152.0	269	28.10
				H	0.029110	0.002950	9.0	3481	27.80
Gl 320	6.32	K1 V	11.14	S	0.460300	0.046610	216.0	505	28.61
				P	0.475400	0.023800	1128.0	921	28.63
				F	0.144100	0.006420	3700.0	3562	28.81
Gl 325A	8.43	K5 V	11.43	S	0.059010	0.014350	25.0	423	27.74
Gl 370	7.43	K5 V	11.15	H	0.006027	0.001050	5.2	7168	27.33
Gl 380	8.15	K7 V	4.87	S	0.176800	0.021330	153.0	494	27.48
				P	0.160100		584.0	3296	27.44
Gl 414A	7.96	K8 V	11.93	S	0.046070	0.015680	10.0	317	27.67
				H	0.006124	0.001510	4.6	3517	27.40

Table 2: Continued

Catalogue Name	M_V	Spectral Type	Distance (pc)	Mode	Count Rate	Error	Likelihood or S/N	Exposure Time	log L_x
Gl 432A	6.06	K0 V	9.54	H	0.003167	0.000877	3.8	6478	26.92
Gl 451A	6.64	G8 VI	9.16	P	0.005465	0.001690	8.0	2765	26.52
Gl 453	6.94	K5 V	10.19	H	0.014320	0.001290	11.2	9483	27.63
Gl 488	8.33	M0.5Ve	10.78	S	0.061280	0.020860	12.0	221	27.71
Gl 505A	6.34	K1 V	11.23	S	0.142800	0.026870	48.0	279	28.11
				P	0.209100	0.011400	1338.0	1656	28.28
				F	0.040800	0.003290	315.0	3634	28.27
Gl 542	6.29	K3 V	11.83	H	0.009136	0.002100	3.2	2445	27.56
Gl 566B	7.82	K4 V e	6.70	S	2.440000	0.183400	416.0	400	28.90
				P	2.351000	0.020700	9999.0	5213	28.88
				F	0.604100	0.011900	9999.0	4270	28.99
				H	0.767300	0.017400	32.7	2495	29.00
Gl 570A	6.90	K5 V e	5.90	S	0.173100	0.070810	9.0	44	27.64
				P	0.238000		1305.0	5321	27.77
				H	0.040760	0.004130	9.4	2443	27.61
Gl 617A	8.45	M0 V e	10.69	S	0.059910	0.007541	91.0	1726	27.69
				H	0.009817	0.001580	5.9	4503	27.51
Gl 631	5.80	K0 V e	9.78	S	0.257900	0.031920	148.0	603	28.25
Gl 638	8.16	K7 V	9.77	S	0.026230	0.009423	11.0	468	27.25
Gl 653	7.57	K7 V	10.76	H	0.002910		7.4 ¹	2213	26.99
Gl 663AB	6.16	K1 V e	5.99	S	0.854100	0.057780	664.0	291	28.34
				P	1.171000	0.025700	9999.0	1783	28.48
				F	0.265100	0.013900	3394.0	1429	28.53
				H	0.146100	0.008600	14.2	1973	28.18
Gl 664	7.46	K5 V e	5.97	S	0.254600	0.031500	157.0	288	27.81
				P	0.265000	0.012800	2360.0	1665	27.83
				F	0.050210	0.006150	165.0	1391	27.81
				H	0.043430	0.005410	4.9	1972	27.65
Gl 667AB	6.99	K3 V	7.25	S	0.205700	0.028810	120.0	307	27.89
				H	0.035800	0.004370	7.7	1916	27.73
Gl 673	8.10	K7 V	7.72	S	0.090570	0.018050	40.0	445	27.59
Gl 688	6.37	K3 V	10.71	S	0.048270	0.013440	19.0	440	27.60
Gl 702B	7.48	K5 V e	5.09	S	1.649000	0.127200	410.0	347	28.49
				F	0.247300	0.011500	4242.0	1903	28.36
				H	0.210900	0.016400	11.0	778	28.20
Gl 706	6.17	K2 V	11.10	H	0.002579	0.000815	4.0	6294	26.96
Gl 713B	6.59		8.06	S	0.155800	0.009018	506.0	2629	27.86
				P	0.152800	0.006840	2255.0	3490	27.85
Gl 764	5.88	K0 V	5.77	S	0.255700	0.014290	694.0	1448	27.79
				P	0.171300	0.008160	2348.0	2684	27.61
				H	0.036140	0.006330	4.9	923	27.54
Gl 773.6	8.35	K5 V	11.80	S	<0.02880		1.5	307	27.45
Gl 783A	6.41	K3 V	6.05	P	0.027630	0.004230	72.0	1883	26.86
				H	0.006246	0.001100	5.4	6530	26.82
Gl 785	6.00	K0 V	8.82	S	0.061820	0.026730	10.0	126	27.54
Gl 820A	7.50	K5 V	3.50	S	0.421700	0.030030	452.0	543	27.57
				F	0.057470	0.003430	1282.0	4934	27.40
				H	0.071220	0.003280	24.2	6688	27.40
Gl 820B	8.32	K7 V	3.50	S	0.421700	0.030030	452.0	543	27.57
				F	0.057470	0.003430	1282.0	4934	27.40
				H	0.024390	0.001960	11.4	6688	26.93
Gl 845	6.89	K5 V e	3.63	S	0.260400	0.028540	169.0	414	27.39
				P	0.507900	0.006080	9999.0	14198	27.68
				F	0.081000	0.004290	2792.0	4410	27.58
				H	0.057770	0.005510	9.3	1958	27.34
Gl 879	7.07	K5 V e	7.64	S	0.526300	0.065160	185.0	150	28.34
Gl 884	8.34	K5 V	8.14	S	<0.11527		6.3	49	27.39
Gl 892	6.50	K3 V	6.53	S	0.023110	0.008761	10.0	497	26.85
Gl 902	6.81	K3 V	11.40	S	0.029190	0.010000	12.0	462	27.44

Table 2: Continued

Catalogue Name	M_V	Spectral Type	Distance (pc)	Mode	Count Rate	Error	Likelihood or S/N	Exposure Time	log L_x
GI 909A	6.24	K3 V	10.79	S	0.419100	0.024660	795.0	747	28.54
LTT 14084	6.50	K3 V	10.10	S	0.016520	0.006606	9.0	813	27.08

Table 3: Sample stars with absolute magnitude fainter than 8.50 and a distance up to 6 pc, M-type stars; columns as in Tab. 1.

Catalogue Name	M_V	Spectral Type	Distance (pc)	Mode	Count Rate	Error	Likelihood or S/N	Exposure Time	log L_x
GI 1	10.35	M3 V	4.36	S	0.059340	0.024300	9.0	156	26.91
				P	0.019690	0.002380	104.0	4604	26.43
GI 15A	10.32	M1.5 V	3.57	S	0.260200	0.026180	202.0	453	27.38
				H	0.013900	0.003060	4.4	1606	26.71
GI 15B	13.29	M3.5 V	3.57	S	0.260200	0.026180	202.0	453	27.38
				H	0.053440	0.005780	8.7	1606	27.29
GI 34B	8.64	K7 V	5.95	S	0.137900	0.021990	71.0	381	27.54
				H	0.026470	0.002070	10.2	6391	27.43
GI 54.1	14.19	M4.5 V	3.72	S	0.253800	0.025840	200.0	461	27.40
				P	0.079810	0.008050	142.0	1359	26.90
GI 65AB	15.41	M5.5 V	2.68	S	0.680300	0.056820	318.0	484	27.55
				P	0.355700		3253.0	16136	27.26
				H	1.410000	0.010100	121.7	13884	28.46
GI 83.1	14.03	M4.5 V	4.45	S	0.167400	0.024950	111.0	295	27.38
GI 166C	12.69	M4.5 V	5.04	S	0.796400	0.051660	572.0	344	28.16
				H	0.107100	0.010400	9.8	1022	27.89
GI 169.1A	12.34	M4 V	5.51	P	0.011920	0.002220	41.0	3323	26.41
GI 191	10.88	M1 p V	3.92	S	0.048740	0.019720	10.0	248	26.73
				P	0.018180	0.001320	353.0	14268	26.30
GI 205	9.19	M1.5 V	5.69	S	0.196300	0.022530	152.0	455	27.66
				P	0.187000	0.006120	2014.0	5156	27.64
GI 213	12.70	M4 V	5.79	S	0.016150	0.006921	9.0	461	26.59
				P	0.004701	0.000729	43.0	13362	26.05
GI 229AB	9.34	M1 V	5.77	S	0.053500	0.011580	39.0	592	27.11
GI 234AB	13.08	M4.0 V	4.12	S	0.767000			490	27.97
GI 251	11.31	M3 V	5.52	P	0.005924	0.001500	30.0	4048	26.11
GI 273	11.95	M3.5 V	3.80	S	0.034000	0.014910	9.0	247	26.55
				P	0.010390	0.002310	37.0	2932	26.03
GI 285	12.30	M4 V	5.93	S	1.467000	0.078880	1220.0	253	28.57
GI 300	13.22	M3.5 V	5.89	P	0.007263	0.001580	28.0	4096	26.26
GI 388	10.95	M3 V	4.89	S	3.701000	0.194400	1500.0	104	28.80
				P	2.226000	0.013500	9999.0	25092	28.58
				H	0.698700	0.006710	94.6	15302	28.68
GI 406	16.56	M6 V	2.39	S	0.227500	0.025720	183.0	384	26.97
				P	0.250000	0.009960	2566.0	2604	27.01
GI 411	10.46	M2 V	2.55	S	0.167000	0.024170	83.0	341	26.89
				P	0.212400	0.004760	3844.0	10006	27.00
GI 412A	10.34	M1 V	4.83	S	0.184800	0.026840	111.0	364	27.49
				H	0.005208	0.000526	5.0	24751	26.54
GI 412B	15.99	M5.5 V	4.83	S	0.184800	0.026840	111.0	364	27.49
				H	0.042180	0.001320	25.4	24751	27.45
GI 445	12.14	M3.5 V	5.39	P	0.021170	0.004150	41.0	1485	26.65
GI 447	13.50	M4 V	3.34	S	0.079610	0.017270	41.0	364	26.80
				P	0.052780		174.0	3885	26.63
GI 473AB	14.99	M5.5 V	4.39	S	0.238600	0.026880	147.0	430	27.52
				P	0.295600	0.012900	2437.0	1922	27.61
GI 526	9.80	M1.5 V	5.43	P	0.035310	0.007460	36.0	747	26.87
GI 551	15.48	M5.5	1.29	S	1.374000	0.110700	445.0	374	27.22
				P	0.541100	0.005680	9999.0	17157	26.81
GI 570BC	9.35	M1 V	5.90	F	0.930500	0.035500	9999.0	725	27.74
				S	0.173100	0.070810	9.0	44	27.64

Table 3: Continued

Catalogue Name	M_V	Spectral Type	Distance (pc)	Mode	Count Rate	Error	Likelihood or S/N	Exposure Time	log L_x
				P	0.238000		1305.0	5321	27.77
				H	0.028530	0.003470	7.4	2443	27.46
G1 570D		T8	5.90	H	<0.00158		1.3 ¹	2430	26.20
G1 588	10.44	M2.5 V	5.93	S	0.039920	0.012640	13.0	416	27.00
				P	0.026350		61.0	4331	26.82
G1 628	11.93	M3 V	4.26	S	0.047450	0.011080	27.0	554	26.79
G1 674	11.10	M3 V	4.54	S	0.266600	0.040960	76.0	193	27.60
G1 682	12.45	M4.5 V	5.04	P	0.007986	0.002780	8.0	1433	26.16
G1 687AB	10.88	M3 V	4.53	S	0.062050	0.004069	374.0	5788	26.96
				P	0.062300	0.003340	1259.0	6274	26.96
				H	0.020350	0.001200	15.3	15193	27.08
G1 693	11.93	M3.5 V	5.81	S	<0.03522		0.7	129	26.93
G1 699	13.25	M4 V	1.82	S	0.029760	0.011060	13.0	399	25.85
				P	0.023370	0.002620	105.0	4127	25.74
G1 725AB	11.14	M3 V	3.56	S	0.049080	0.006292	91.0	1781	26.65
				P	0.062860	0.005710	158.0	2263	26.76
				H	0.021700	0.002330	8.3	4178	26.90
G1 729	13.09	M3.5 V	2.97	S	0.942000	0.080930	334.0	326	27.78
				H	0.204200	0.006880	27.5	4305	27.71
G1 752A	10.28	M3 V	5.87	P	0.035360		139.0	10492	26.94
				H	0.011460	0.000778	14.6	21758	27.05
G1 752B	18.68	M8 V	5.87	H	0.000444	0.000323	3.0	21757	25.64
G1 754	13.41	M4.5	5.71	P	0.004324	0.000974	15.0	6529	26.01
G1 825	8.70	M0.5 V	3.95	S	0.137300	0.022020	83.0	403	27.19
				P	0.248600	0.005250	3589.0	9467	27.44
G1 832	10.20	M1 V	4.94	P	0.033740	0.004580	54.0	2041	26.77
G1 860AB	11.76	M3 V	4.04	S	0.448600	0.033550	468.0	427	27.72
G1 866AB	15.18	M5 V	3.45	S	0.196900	0.038900	57.0	161	27.23
				P	0.269900	0.004640	3800.0	12892	27.36
G1 873	11.71	M3.5 V	5.05	S	5.384000	0.098370	9999.0	560	28.99
				P	0.784500		5458.0	4463	28.16
G1 876	11.80	M3.5 V	4.70	P	0.019320	0.003770	34.0	1766	26.49
G1 887	9.76	M2 V	3.29	S	0.137400	0.037470	28.0	148	27.03
				P	0.222000	0.004350	3425.0	12729	27.24
G1 905	14.79	M5.5 V	3.16	S	0.177200	0.023810	100.0	350	27.10
G1 908	10.11	M1 V	5.97	S	0.051160	0.013450	27.0	414	27.12
GJ 1002	15.40	M5.5 V	4.69	P	<0.00219		0.3	1673	25.54
GJ 1005AB	12.99	M3.5 V	5.36	P	0.007931	0.002540	10.0	1643	26.21
GJ 1061	15.17	M5.5 V	3.70	P	0.011900	0.003690	16.0	1321	26.07
GJ 1111	16.99	M6.5 V	3.63	P	0.039730		264.0	10312	26.58
GJ 1116AB	15.48	M5.5 V	5.23	S	0.340000	0.034000	231.0	337	27.82
				P	0.171700		389.0	3021	27.53
				H	0.070920	0.003670	17.9	5319	27.75
GJ 1245ABC	15.18	M5.5 V	4.54	S	0.198200	0.016990	331.0	797	27.47
				H	0.026270	0.003120	6.8	2849	27.19
LHS 288	15.61	M5.5	4.49	P	0.197300	0.016300	302	730	27.46
				H	0.00079	0.00028	11.7 ¹	12927	25.66 ²
LHS 292	17.32	M6.5 V	4.54	P	0.006161	0.001330	39.0	5146	25.96
LP 71-82	14.43	dM7 e	5.00	S	0.143900	0.004378	2290.0	9529	27.41
LP 816-60	12.71	M	5.49	S	<0.02430		1.9	326	26.72
LP 944-20	18.25	M9 V	4.97	H	<0.00415			220800	25.57 ³
LTT 17897	12.69	M3.5 V	5.37	S	0.404000	0.044720	193.0	475	27.92
L 34-26	12.90	dM5 e	5.99	S	0.594400	0.070090	171.0	753	28.18
DENIS 1048-39	18.50	M9 V	4.10	S	<0.01599		0.5	409	26.29

¹ Given value is the source likelihood² Source not included in the HRI catalog. See Sec. 5.4.2 for details.³ X-ray data taken from Neuhäuser et al. (1999)

Distribution of PSPC Pointing and survey count rates

